Arch. Metall. Mater., Vol. 61 (2016), No 3, p. 1655–1662

DOI: 10.1515/amm-2016-0268

J. MICHALCZYK*#, M. NABIAŁEK*, M. SZOTA*

MATHEMATICAL MODELLING OF THERMO-ELASTO-PLASTIC PROBLEMS AND THE SOLVING METHODOLOGY ON THE EXAMPLE OF THE TUBULAR SECTION FORMING PROCESS

The paper presents the results of numerical studies based on a mathematical model determined by the stress-strain state examination method. Numerical computations for two steel grades, namely H40 and C45, were made at similar strain and process rate parameters. As a result of the studies, the distribution of elastic and plastic zones was obtained, while the tube hollow drawing force was verified experimentally. The distribution of longitudinal, radial and circumferential stresses and, after the drawing operation, the distribution of residual stresses in the tube cross-section were also obtained.

1. Introduction

The notion of mathematical model is understood as any equation derived by an empirical or other method, which describes only the variation of a single arbitrary criterion, depending on the process parameters, and not an arbitrary simplified engineering methodology for calculating the force, but instead a set of mathematical equations describing any, even the tiniest variations in the behaviour of the material being worked, for all possible (and even unknown yet) changes in the process parameters [1,9].

Creation of these models should be based on basic sciences, such as continuous medium mechanics, solid-state physics, numerical methods and materials science. Such models normally consist of packages of programs designed for contemporary computers [10].

The theoretical analysis of metal plastic working processes should include the definition and determination of the distributions of metal particle velocities, strain rates, strains and stresses; the distributions of unit pressures on the metal-tool contact surface; and the determination of the force and energy process parameters and the quality and strength indices [2, 3]. The final stage of the comprehensive analysis must include the optimization of the plastic working process. Mathematical analysis is a basis for the optimization of technological processes and requires the solution of very complex equations of relationships between particle displacements and strains, and stresses [6].

Considering the strain hardening of metals during working, the complex shape of the deformation zone and the significant effect of the variation of temperature and speed in the equations requires non-linear problems to be solved. The non-linear problems can be provisionally solved only by introducing a series of simplifications or using numerical methods [7,11].

When examining the above-mentioned methods of analyzing plastic working processes it can be noticed that none of them includes the complete analysis of the technological process. During the course of analysis one must determine the stress and strain state and the strain and displacement rates, while allowing for temperature effects variable in time (loading history), some indices of mechanical properties, the use of the plasticity reserve, the distribution of elastic and plastic zones, residual stresses, etc. The possibility of controlling the mechanical properties of stock and product during plastic working and the obtaining of the required mechanical properties, residual stresses and macro- and microstructure are the main problems of plastic working.

In order to solve these problems, mathematical models of the technological processes should be available, which will describe the basic deformation features, while considering the history of loading of each metal particle. Mathematical modelling must be universal in terms of applicability to different plastic working processes [6, 7]. Developing such a mathematical model requires a plane or axially-symmetrical thermal–elastic–plastic problem to be set up and solved under complex loading conditions. This involves issues related to the selection of defining relationships, the accuracy of results to be obtained, the methods of numerical solving of equations, the need for taking account of the elastic and viscous properties in the deformation of metals, the thermal effects, the selection of an optimal mesh of elements and its transformation in the deformation process, etc. The Compromiss, a commercial software package, was used for computation [1].

2. Problem solving algorithms

Shown below is a methodology for solving the thermal–elastic–plastic tasks using the basic equations of the finite-element method. First, the algorithm for solving a non-stationary task is considered. The entire range is broken up

* CZĘSTOCHOWA UNIVERSITY OF TECHNOLOGY, FACULTY OF PRODUCTION ENGENIERING AND MATERIALS, 19 ARMII KARAJOWEJ STR, 42-200 CZĘSTOCHOWA, POLAND
# Corresponding author: jm.@wip.pcz.pl

into a series of sufficiently small stages (steps). The solution algorithm consists of the following points:

1. The region under study, corresponding to the moment t = 0 and being an unknown, is approximated with a finite-element grid. Based on the known initial stresses, the elastic and plastic deformation zones are determined in the zero approximation in the first step. According to the known configuration, the contact zones and the free surfaces are defined.
2. The heat conduction boundary task with preset boundary conditions and heat sources is solved (in the first iteration of this step, the power of the sources from plastic deformation and boundary friction is assumed to be equal to zero). The methodology for solving the heat conduction boundary task is shown in study [10]. On the basis of the solution of the heat conduction task, the temperature field is determined for an arbitrary moment of a given loading step.
3. Bases on the known $\dot{\theta}(\rho,z),\theta(\rho,z)$, initial stresses, strains and boundary conditions, the coefficients of the system of quasi-linear algebraic equations and its right-hand side are determined. By solving the system, we calculate the nodal rates of displacements, strains and stresses in each element.
4. Using the determined displacement rates and initial conditions for the displacements, we determine the displacement field, based on which, in turn, the strain tensor components are found.
5. The elastic and plastic deformation zones, the contact region boundaries and the heat sources are specified. It must be borne in mind here that the thermal–elastic–plastic task being solved is physically nonlinear. However, by using this methodology, the linearization of tasks is made in each iteration, which enables in such a case a system of linear algebraic equations to be solved. To this end, the secant module method is used, whose idea relies on the use of the single curve hypothesis and the experimental dependence of the yield stress of the examined material on the strain, strain rate and temperature. In each iteration, we convert the matrix of properties [l] for all elements occurring in the plastic strain region. The iteration process is carried on up to the point in which the plasticity conditions are not satisfied with the assumed accuracy for all plastic elements. Then, the convergence conditions of the iteration process are verified (from the condition of the minimum difference of displacement rates, displacements and stresses in two adjacent iterations in space). In the case where convergence conditions are not satisfied, points 2÷5 are executed until the assumed accuracy has been attained.
6. The configuration and the position of nodal points corresponding to the end of the loading step, as well as the fields of stresses, strains and temperatures are determined. This is followed by the transition to a new loading stage. Note, that the displacements, stresses and temperatures of the last iteration of the n-th loading step are the initial conditions for the loading stage (n+1).

With the above methodology, also stationary tasks can be solved using the stabilization method (the solution of the non-stationary task to go out to the state of stationarity). However, the execution of this method involves a considerable elongation of the computation time. Therefore, in order to solve stationary tasks, a methodology relying on the Euler–Lagrange approach has been developed. The idea of this approach lies in the tracking of the motion of material particles through the finite-element grid rigidly tied with the readout system (a conventionally immovable coordinate system). Let us note that, in the case of a steady metal flow, the trajectories of material particles coincide with the flow lines.

Although neither the flow lines, nor elastic and plastic strain zones, nor contact lines are known a priori, the solution algorithm is iterative.

In the zero approximation it is assumed that the spatial region under examination, filled up with the material, is limited by the surface of the deforming tool in the geometric deformation zone, the approximately assumed stock and finished product surfaces, and some entrance surfaces in the real deformation region.

Assume that, inside the region limited by these planes, the mechanical state of the material is invariable.

Thus defined spatial region is approximated with a finite-element grid, with the flow lines in the zero approximation being determined by proportionally dividing segments in the direction of the axis perpendicular to the metal flow direction. At the same time, elements located between two adjacent flow lines, being in motion and moving in time Dt, are successively replaced by the same particles.

3. The method of the study of the stress–strain state of the processes of working of materials in a steady stage

Assume that the flow vector lines are known for the metal flow process under study. For the plastic region, the physical relationships have the form of small-curvature process equations:

$$S_{ij} = 2\mu\xi_{ij}, \tag{2.1}$$

where; ξ_{ij} – components of the strain rate tensor.

If the volume change in plastic deformation is neglected, then the relationships (2.1) correspond to the incompressibility equation:

$$\xi_{kk} = 0. \tag{2.2}$$

In the elastic zone, the physical relationships are written in the following form:

$$\Delta S_{ij} = 2G\Delta e_{ij}, \tag{2.3}$$

where, $\Delta e_{ij} = \xi_{ij}\Delta t$ - increment in the strain deviator components in a very short time $\Delta\tau$.

The volume change equation is also represented using increments:

$$\Delta\sigma = K\Delta\varepsilon,\ K = \frac{E}{1-2\mu}. \tag{2.4}$$

By introducing the modules $G^{'} = G\Delta t$ and $K^{'} = K\Delta t$, Eq. (2.3) and Eq.(2.4) can be written in the form of linearly-viscous continuum equations:

$$\Delta S_{ij} = 2G^{'}\xi_{ij}; \tag{2.5}$$

$$\Delta\sigma = K^{'}\xi,\ \ \xi = \frac{1}{3}\xi_{ii}. \tag{2.6}$$

Then, using the equilibrium equations (for the elastic zone, the equilibrium equations have been written using stress increments, while in the plastic zone, in the form of total stresses), the physical equations (2.1), (2.2) and (2.5), (2.6), and the Galerkin method, solving FEM equations can be obtained in the following form:

$$\left[K\right]\left\{\begin{matrix}V\\ \sigma\end{matrix}\right\}^{\vee} = \left\{F\right\}. \tag{2.7}$$

The unknowns searched for are here the meanings of the components of the vector of displacements velocities along the coordinate axis $\left\{V\right\}$ and the mean stress magnitude $\left\{\sigma\right\}$ in each of the nodes. As neither the shape of the free surface, nor the flow lines, nor the plastic and elastic strain zones are known a priori (by assumption), the following iteration procedures are used for their determination.

In the zero approximation it is assumed that the examined region is limited by the tool surface in the geometrical strain region zone and, in approximation, by the preset preform and finished product surfaces (Fig. 2.1).

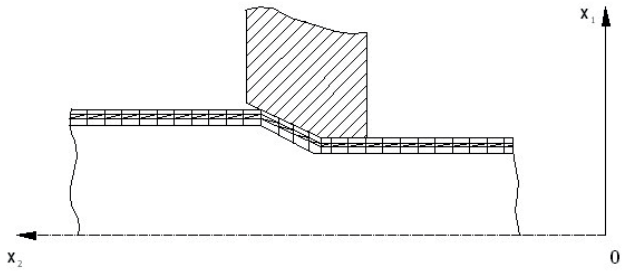

Fig. 2.1. Schematic diagram of the region under examination

The flow line in the zero approximation are defined by the proportional division of segments in the direction of the OX_1 and OX_2 axes. In the zero approximation we assume that the entire examined region is in an elastic state.

Using the physical relationships (2.5) and (2.6), the fields of displacement and strain rates have been determined from Eq. (2.7). Assuming that all elements are in motion along the flow line, and by integrating along the flow line, the strain rates can be determined.

On the assumption of the smoothness of the strain rate field and the short time of the displacement of elements to adjacent positions, the integration can be substituted with summing:

$$\varepsilon_{ij}^{(m)} = \sum_{n=1}^{m-1}\xi_{ij}^{(n)}\Delta t^{(n)}, \tag{2.8}$$

where: m – number of the element along the flow line;

$\Delta t^{(n)} = \dfrac{l_1^{(n)}}{V_x^{(n)}}$ – time of element displacements from the position n to the positions n+1;

$V_x^{(n)}$ – longitudinal velocity of the centre of gravity at the n–th element.

Based on the determined strains $\varepsilon_{ij}(\vec{x})$ and strain intensities $\varepsilon_i(\vec{x})$, the elastic strain zones (including weakening zones) and the plastic strain zones are determined. For the plastic zones, the secant module of the first approximation is determined. So, the solution is repeatable, whereas, for the elastic zones, Equations (2.5) and (2.6) are used as physical relationships, while for the plastic zones, Equations (2.1) and (2.2) with the determined values of the modules $\mu^{(1)}(x)$.

The iteration process will be finished, if the modules of the maximum differences by elements are smaller than the preset numbers:

$$\max_p\left|\xi_{ij}^{(k)p} - \xi_{ij}^{(k-1)p}\right| < \delta_\xi \text{ and } \max_p\left|\sigma_{ij}^{(k)p} - \sigma_{ij}^{(k-1)p}\right| < \delta_\sigma,$$

where: δ_ξ and δ_σ are small positive numbers.

In that case, for the plastic zone elements, the plasticity condition must be satisfied with the specified accuracy.

Then, by integrating the obtained displacement velocity fields along the flow lines, the flow lines and the free surface position can be corrected. The flow line correction process is finished, if the maximum meaning of the module of the velocity vector component normal to the flow line, by the region, meets the following condition:

$$\max_{\vec{x}\in\Omega}\left|V_{II}(\vec{x})\right| < \varepsilon,$$

where: ε – preset positive value.

As an example, we will use the mathematical modelling method for the analysis of the stress–strain state of the tube hollow cold drawing process.

4. Analysis of the problem on the example of tubular section cold drawing

The steel cylinder cold drawing process with wall thickness reduction was subjected to analysis. The process is analyzed at the steady flow stage [1].

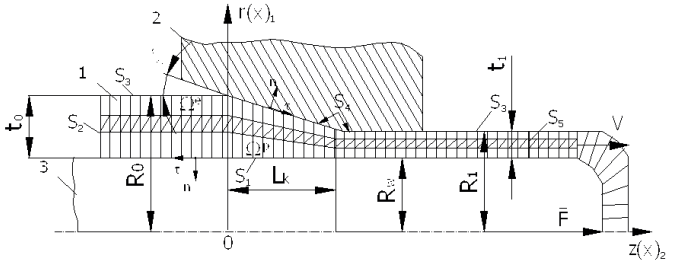

Fig. 3.1. Schematic diagram of the tube hollow drawing process

The drawing scheme is shown in Fig. 3.1. The prepared tube hollow 1 is drawn through die 2. Deformation takes place due to the movement of punch 3, whereas, in some zones situated at a certain distance from the deformation zone output cross-section ($1.5 – 2L_k$, where L_k – conical die portion length), the punch motion velocity and deformed metal motion velocity are identical.

The open domain Ω in the Euclidean space R^3, with the boundary S, is filled with metal that flows under the action of the external force F. The domain Ω is represented as a combination of two sub-domains: the elastic strain sub-domain Ω^e and the plastic strain sub-domain Ω^p. The sub-domain Ω^e contains deformed metal elastic loading and unloading zones. The material in the plastic zone Ω^p is characterized by incompressibility and large strains, and the loading process is close to the simple one (the main axes of the strain tensor and strain rate tensor deviators coincide and remain invariable relative to the metal fibres).

It was presumed that all plastic formation work transformed itself into heat, and half of the heat caused by the friction on the metal-tool contact surface penetrated into the tool.

The region under examination is divided into finite elements. Metal particles move along respective flow lines which coincide with their trajectories. Finite elements move along the flow lines, passing successively one into another after a certain time Dt. At the same time, the stress state in the preceding element is at the beginning of the next one.

The stress–strain state of the metal in this process is axially symmetrical and can be described by geometric relationships in the elastic zone $\left[K^e{}_i\right]\left\{\Delta\delta_i^{(1)}\right\} - \left\{\Delta F^e{}_i\right\} - \left\{R_i^{(0)}\right\} = 0$ and the plastic zone $S_{ij} = 2\mu\xi_{ij}$. Boundary conditions need to be added to these equations, which in the case under consideration have the following form (the designations as per Fig. 3.2).

$$\left.\begin{array}{lll} V_n = 0, & F_\tau = \mu_S F_S & \vec{x} \in S_1 \\ F_r = F_z = 0 & & \vec{x} \in S_2 \oplus S_3 \\ V_n = 0, & F_\tau = \mu_m F_S & \vec{x} \in S_4 \\ F_r = 0, & V_z = \hat{V} & \vec{x} \in S_5 \end{array}\right\}, \qquad (3.1)$$

where: $\vec{F}$ – surface force vector,
$\hat{V}$ – preset velocity drawing,

μ_S and μ_m – friction coefficients on the surface of metal contact with the punch and the die, respectively;

the indexes n and t refer to the normal and tangential components of the respective vectors.

The boundary of the examined region is represented in the form of the simple sum of areas S_i, $S_i = S_1 \oplus S_2 \oplus S_3 \oplus S_4 \oplus S_5$, with parts of the boundaries S_4, S_3 and S_1 are unknowns and are determined during solving from the conditions of the impenetrability and negativity of normal stresses. In addition, note that the elastic and plastic strain zones are also a priori unknown and need to be determined during the course of solving the problem.

In the formulation of the problem using the method mentioned earlier, the stress–strain state was examined for two drawing variants with the following parameters.

1. The material – steel 40H; initial diameter, D_0 = 25 mm; punch diameter, D_w = 17.4 mm; final diameter, D_1= 23.7 mm; elongation factor, $\lambda = \frac{S_0}{S_1} = 253.1/203.4 = 1.24$; die conicity half-angle, $\varphi = 12^0$; coefficient of friction on the metal-die contact surface, μ_m = 0.2, and on the metal-punch contact surface, μ_s = 0.2. Drawing speed, V = 70.5 mm/s.
2. The material – steel 45, D_0 = 94 mm, D_w = 80 mm, D_1 = 92 mm, j = 100, l=1.17, μm = 0.2, m_s = 0.285. V = 152.5 mm/s.

The accuracy of the methodology was verified in drawing a tube hollow of steel 40H. Applied drawing lubricant MoS2. Applied tool - conical die block. The measurement of force the testing machine. According to experimental results, the drawing force was equal to 18.2 kN. According to calculations, the force amounted to 15.52 kN. The deviation is 15%. These discrepancies are due to the inaccurate knowledge of the actual magnitudes of the friction coefficients, and also the metal resistance to deformations under given temperature, strain rate conditions. It should be noted, however, that such a discrepancy in results is acceptable in the study of plastic working processes.

This method is markedly distinguished by the fact that the use of the proposed computations allows the spread of elastic and plastic zones to be determined. Using the traditional methods of the study of the stress–strain state in extrusion, rolling and drawing processes, the plastic zone has normally been separated from the elastic zone with the arcs ab and cd.

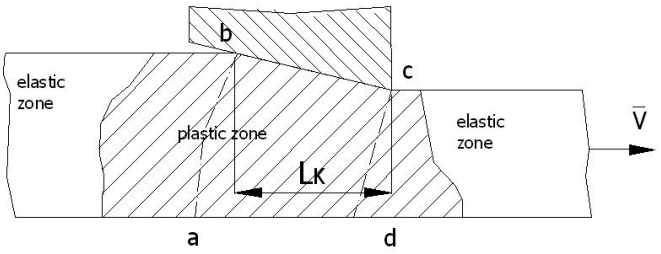

Fig. 3.2. Distribution of elastic and plastic zones in drawing a hollow

Figure 3.2 shows the distribution of elastic and plastic zones obtained by using the new method. The plastic zone exceeds the deformation zone boundary.

The magnitude of this exceeding equals 1.5 L_k at the entry and 2/3 L_k at the exit from the conical die portion (L_k– the length of the conical portion of the deformation zone). These results were verified experimentally by microhardness measurements and by the visioplasticity method.

The diagrams of longitudinal metal velocities are shown in Fig. 3.3. The convexity of the curves varies from the entry to the conical die portion until the exit from this portion.

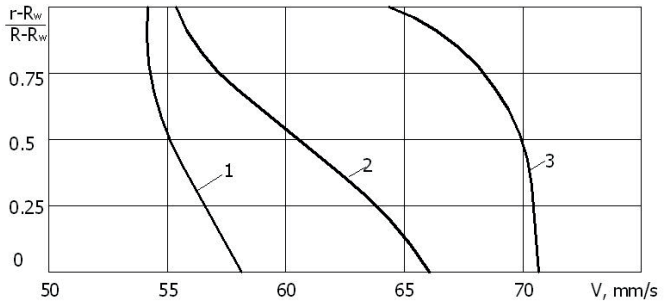

Fig. 3.3. Distribution of longitudinal velocities along the product wall thickness. 1) at the entry, 2) in the centre, 3) at the exit from the conical die portion.). For steel 45. R_w- internal radius, r – external radius

As can be seen from the figure, the maximum metal flow speed occurs in the external zone of the hollow, at the exit from the die deformation zone.

The diagrams of radial velocities are shown in Fig. 3.4.

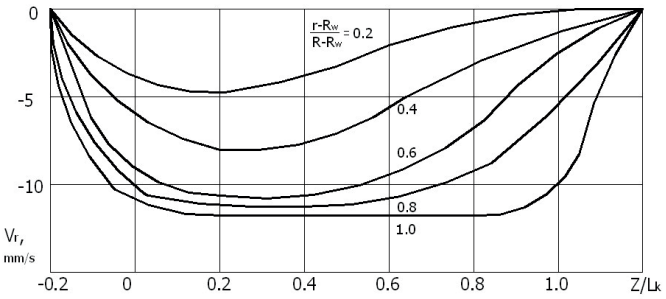

Fig. 3.4. Distribution of radial velocities along the cylinder wall thickness in drawing. (R- current die radius, R_S- punch radius). For steel 45. R_w- internal radius, r – external radius

The radial metal flow velocity increases from the punch surface to the die; however, the radial displacement velocity gradients are maximum at the punch surface. It can be seen from the figure that beyond-contact deformation (so called „draw-in") occurs in the frontal $\frac{z}{L_k} > 1$ and the rear $\frac{z}{L_k} < 0$ outer zones.

The behaviour of the variability of displacement velocities is consistent with those shown in the strain diagrams (Fig. 3.5).

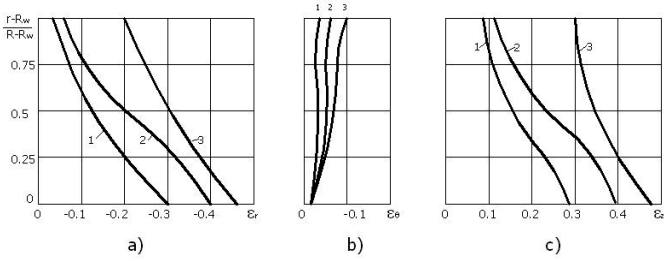

Fig. 3.5. Strain redistribution of along the hollow wall thickness: a) - radial strains, b) - circumferential strains, c) - longitudinal strains. 1) $\frac{Z}{L_K} = 0.1$, 2) $\frac{Z}{L_K} = 0.5$, 3) $\frac{Z}{L_K} = 1.0$. R_w- internal radius, r – external radius. For steel 45

The radial strains and the longitudinal strains attain a maximum on the punch contact surface, which is determined by the action of friction forces on this surface.

The largest circumferential strains are observed on the metal-die contact surface, as it is on this surface that the maximum radial metal flow velocity occurs. In total, the circumferential deformation is much smaller than the radial and longitudinal deformations, which is explained by the considerable magnitude of the radii of the layer of metal existing in the hollow wall, relative to the radial displacements.

Figure 3.6 illustrates the variation of equivalent strain. Both the strain intensity ei and the strain tensor components have larger values on the metal-tool contact surface .

The degree of utilization of the plasticity reserve $\varphi = \frac{R_e}{R_m}$ – also has its maximum value on the inner surface of the metal being deformed (Fig. 3.6).

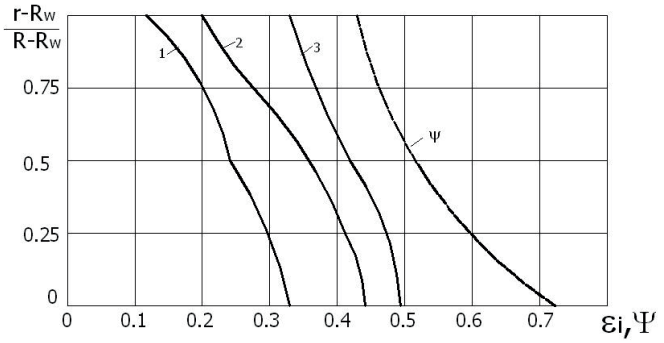

Fig. 3.6. Variation of strain intensity ε_i (1,2,3) and the degree of utilization of the plasticity reserve ψ along the hollow wall thickness. 1) z/l_k=0.1; 2) z/l_k=0.5; 3) z/l_k=1.0 For steel 45

Figures 3.7 and 3.8 represent the diagrams of the distribution of stresses on the metal contact surfaces for two variants under consideration. Variant with the punh and variant with die block. The stress distribution behaviour in these cases is practically the same. The radial stress on the metal-die contact surface has two maximum values, namely, at the entry to, and at the exit from the deformation zone, which is consistent with the experimental and theoretical study results obtained by the authors of the paper.The appearance of two maxima is due to the intensive change in the direction of metal flow around the entry and exit cross-sections in the conical die portion in these regions of elastic (dead) stress zones.

On the die block-metal contact surface, the stress components show a monotonic behaviour, with the sq i sr increasing from the cross-section of entry to the cross-section of exit from the conical die portion, while the sz reduction.

It can be noticed that, if overall compression takes place in the metal-die contact zone, then in the metal-punch contact zone the stress has different signs. This explains the appearance of the large degree of deformation in the internal layers of the cylindrical preform compared to the external layers. In the cylindrical sizing portion of the die, the circumferential and radial stresses on the external surface decrease almost to zero, and the longitudinal stresses change their sign (Fig. 3.8).

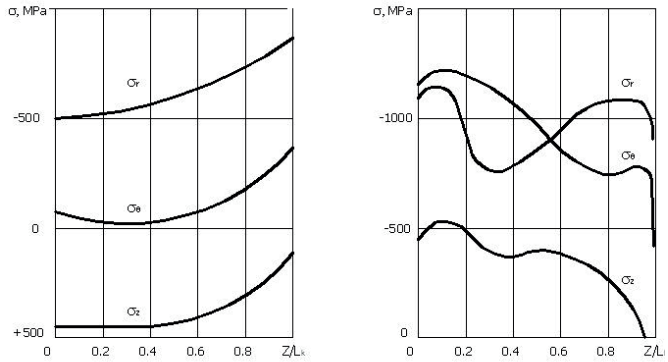

Fig. 3.7. Stresses on the surface of contact of the preform during production of a hollow: a) with the punch, b) with the die. For steel 45

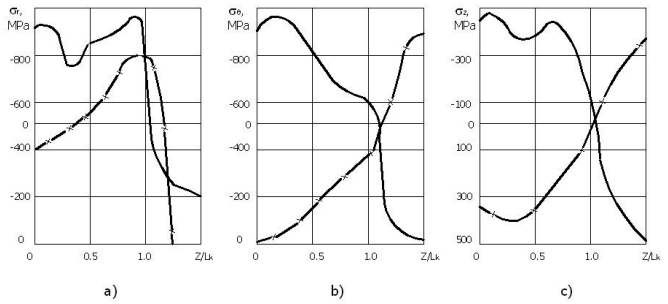

Fig. 3.8. Variation in stresses on the surface of contact with the die (--) and the punch (-x-x) during cold hollow drawing; a) radial, b) circumferential, c) longitudinal For steel 45

The equivalent stress at the exit from the conical die portion is increased in the direction from the internal surface to the external surface of the hollow (Fig. 3.9).

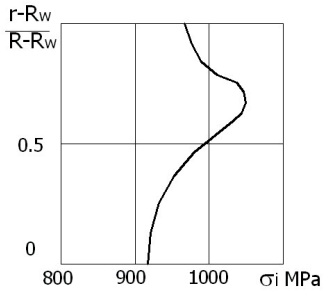

Fig. 3.9. Variation in stress intensity along hollow wall thickness (z/l_k=1.1). For steel 45

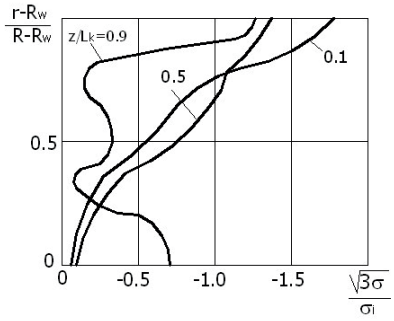

Fig. 3.10. Variation in the state of stress relative to hollow wall thickness For steel 45

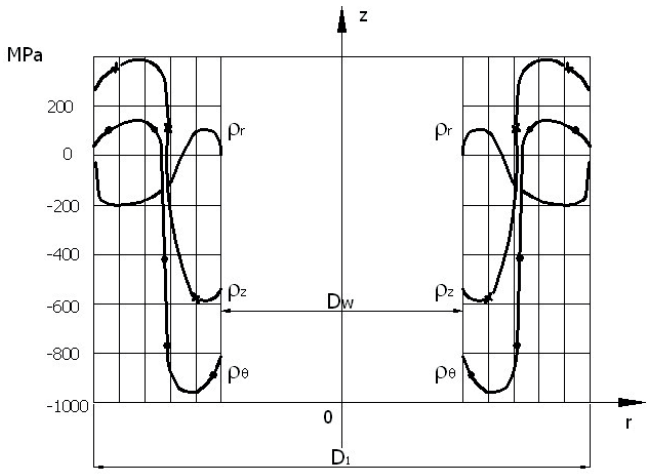

Fig. 3.11. Distribution of residual stresses in the walls of the hollow after cold drawing. For steel 45

The difference in equivalent stress along wall thickness is about 15% of the yield point of the steel in the finished product.

The stress state index $\frac{\sqrt{3}\cdot\sigma}{\sigma_i}$ characterizes the plasticity reserve of the metal (for both steel 40H and steel 45, the plasticity reserve increases with the decrease in this index). On the external surface of the hollow, the stress state index increases with increasing reduction, while on the internal surface, the index decreases (Fig. 3.10).

5. 4. Conclusions

As a result of solving the problem with unloading, diagrams of residual stresses in the finished product were obtained (Fig. 3.11). The longitudinal residual stresses are compressive in the region $1 \le \frac{r-R_0}{R_1-R_0} \le 3$ and tensile in the last portion of the cross-section. The obtained stress distribution behaviour is in total consistent with the longitudinal strain diagrams: large internal fibre plastic deformations, which occur in the drawing process upon unloading, cause the compression of these tensioned fibres, as the total deformation is constant relative to the cross-section.

In a similar way, the appearance of the internal tensile stresses in the region adjacent to the external hollow surface can be explained. The behaviour of the variation in the external, stresses internal is similar to the distribution of longitudinal stresses. The radial residual stresses are equal to zero on the free surfaces, being tensile in external hollow layers and compressive in internal hollow layers. The resemblance behaviour of the variation in Distribution of ρ_θ and ρ_r can be explained as follows. The compressive stresses in the radial and circumferential directions of the metal layer tend to widening upon exit from the die, with the radial stresses in the external metal layers being compressive, while the circumferential ultimate stresses restricting the metal widening being tensile. The widening of the internal layers of the hollow upon exit from the die and after unloading leads to the appearance of radial tensile and circumferential compressive internal stresses in the internal layers of the hollow wall. The most

disadvantageous from the point of view of the performance of the finished product is the distribution of ultimate stresses in the region adjacent to the external hollow surface. To reduce the harmful effect of ultimate stresses, as well as other factors, on the quality of the hollow, the process of optimization of the technological process should be employed.

REFERENCES:

[1] V.V. Dewiatov, H.S. Dyja, V.Y. Stolbow: Modeling mathematical and optimization processes extrusions, Częstochowa 2004.

[2] V.V. Dewiatov, J. Michalczyk: The method production sleeves deep from bottom. Polish Patent 206468.

[3] V.V. Dewiatov, J. Michalczyk, Z. Potęga: Determination of methodology internal stresses for example calibration bar. Technical education and informatics. Scientific work - Academy. Jan Długosz in Częstochowa (2008).

[4] A.A. Il'jushin: Mehanika sploshnoj sredy. Moskwa 1978.

[5] Ju. I. Njashin, V.V. Devjatov, V.Ju. Stolbov, R.M. Podgaec: Issledovanie temperaturnyh polej v processah prjamogo vydavlivanija sploshnyh cilindrov. Chernaja metallurgija (1987).

[6] J. Michalczyk, T. Bajor: Archives Metallurgy and Materials **56**, 553-541 (2011).

[7] J. Michalczyk: Archives Metallurgy and Materials **58**, 133-137 (2013).

[8] J. Piwnik: The Modeling processes plastic flow. Białystok 1992.

[9] M. Pietrzyk: The numerical methods in plastic working metals. Kraków 1992.

[10] G. Samołyk: Archives Metallurgy and Materials **58**, 1143-1189 (2013).

[11] P. Szota, A. Stefanik., Dyja H.: Archives Metallurgy and Materials **54**, 607-615 (2009).